© The American Society of Gene & Cell Therapy

Bevacizumab With Angiostatin-armed oHSV Increases Antiangiogenesis and Decreases Bevacizumab-induced Invasion in U87 Glioma

Wei Zhang[1,2], Giulia Fulci[1], Jason S Buhrman[1], Anat O Stemmer-Rachamimov[3], John W Chen[4], Gregory R Wojtkiewicz[4], Ralph Weissleder[4], Samuel D Rabkin[1] and Robert L Martuza[1]

[1]Brain Tumor Research Center, Department of Neurosurgery, Massachusetts General Hospital, Boston, Massachusetts, USA; [2]Department of Neurosurgery, Xijing Hospital, The Fourth Military Medical University, Xían, People's Republic of China; [3]Department of Pathology, Massachusetts General Hospital, Boston, Massachusetts, USA; [4]Center for Systems Biology and Molecular Imaging Research, Massachusetts General Hospital, Boston, Massachusetts, USA

Bevacizumab (BEV) is an antiangiogenic drug approved for glioblastoma (GBM) treatment. However, it does not increase survival and is associated with glioma invasion. Angiostatin is an antiangiogenic polypeptide that also inhibits migration of cancer cells, but is difficult to deliver. Oncolytic viruses (OV) can potentially spread throughout the tumor, reach isolated infiltrating cells, kill them and deliver anticancer agents to uninfected cells. We have tested a combination treatment of BEV plus an OV expressing angiostatin (G47Δ-mAngio) in mice-bearing human GBM. Using a vascular intracranial human glioma model (U87) in athymic mice, we performed histopathological analysis of tumors treated with G47Δ-mAngio or BEV alone or in combination, followed tumor response by magnetic resonance imaging (MRI), and assessed animal survival. Our results indicate that injection of G47Δ-mAngio during BEV treatment allows increased virus distribution, tumor lysis, and angiostatin-mediated inhibition of vascular endothelial growth factor (VEGF) expression and of BEV-induced invasion markers (matrix metalloproteinases-2 (MMP2), MMP9, and collagen). This leads to increased survival and antiangiogenesis and decreased invasive phenotypes. We show for the first time the possibility of improving the antiangiogenic effect of BEV while decreasing the tumor invasive-like phenotype induced by this drug, and demonstrate the therapeutic advantage of combining systemic and local antiangiogenic treatments with viral oncolytic therapy.

Received 27 April 2011; accepted 7 August 2011; published online 13 September 2011. doi:10.1038/mt.2011.187

INTRODUCTION

Despite improved understanding of the molecular and physiological features of glioblastoma (GBM), there are no effective treatments for this brain cancer. The average prognosis has not changed by more than a few months over the last 20 years and median life expectancy after diagnosis is ~15 months. Several modalities have been and continue to be tested to treat these tumors, but none of these can extend life for more than a few months.

Antiangiogenic therapy is one of the strategies used to treat GBM. The major disadvantage of most antiangiogenic treatments is the induction of tumor invasion.[1] Bevacizumab (Avastin, BEV), a monoclonal antibody that inactivates vascular endothelial growth factor (VEGF), was recently approved by the US Food and Drug Administration as a single agent for treatment of recurrent GBM.[2] It reduces MRI enhancement, and provides benefit by controlling peritumoral edema and improving clinical performance. Its clinical use is increasing, even though its effect on the overall survival remains poor and it induces nonenhancing tumor invasion.[3,4] It is thus important to test the potential uses of BEV in combination treatments that could improve the therapeutic outcome and decrease the drug's induced tumor invasion.

Angiostatin is an endogenous inhibitor of angiogenesis[5] that was shown to efficiently inhibit growth of primary and metastatic tumors and prolong patient survival (DeMoraes *et al*., 2001, Abstracts of the 37th ASCO meeting). Its antiangiogenic and tumoristatic effects were also observed in preclinical studies for GBM.[6] However, because angiostatin has a very short half-life, it presents important delivery problems[7] and it was never tested in patients with GBM. The full molecular pathway through which angiostatin inhibits angiogenesis is not yet clear, but it was shown to block matrix-enhanced plasminogen activation, thereby inhibiting migration of endothelial, immune and cancer cells.[8,9] Indeed, it inhibits cancer metastasis and invasion.[8,9] We thus hypothesized that the combination of BEV and angiostatin could attack two different angiogenic pathways and lead to an additive antiangiogenic effect without inducing tumor invasion.

Genetically engineered oncolytic herpes simplex viruses (oHSV) are an attractive therapeutic means for treating locally growing, nonmetastatic tumors such as GBM due to their capacity to selectively replicate in tumor cells, lyse them and spread their progeny to the remaining cancer cells.[10] oHSV have the potential to increase *in situ* after delivery and reach isolated infiltrating cancer cells.[11] Moreover, the mode by which oHSV kills cells differs from that of standard anticancer agents and has differing

Correspondence: *Robert L Martuza, Brain Tumor Research Center, Department of Neurosurgery, Massachusetts General Hospital, 55 Fruit Street, Boston, Massachusetts 02114, USA. E-mail: rmartuza@partners.org*

© The American Society of Gene & Cell Therapy

sets of toxicities, thus making them a useful tool for multimodal combination treatments.[12–14] In addition to their oncolytic action, oHSV can be "armed" to express therapeutic genes such as sensitizers to chemotherapy, immune stimulators and inhibitors, and antiangiogenic factors.[11,15–32] However, the overall performance of oHSV as single treatment is poor, due in part to the presence of a host antiviral innate immunity.[15,33–40] We and others have shown that oHSV induce intratumoral infiltration of macrophages that engulf virus-infected cancer cells and inhibit oHSV replication and persistence.[15,33–40] Antiangiogenic treatments prevent intratumoral infiltration of macrophages and increase oHSV replication and spread.[39,41,42]

Given the potential mechanistic synergy existing between the antiangiogenic drug BEV and oncolytic viruses (OV), the possible additive antiangiogenic effect of BEV and angiostatin, and the anti-invasive capacity of angiostatin, we hypothesized that a combination of systemic BEV plus local expression of angiostatin could increase OV treatment efficacy of GBM and decrease BEV-induced invasion. To test our hypothesis, we created G47Δ-mAngio by arming an HSV-derived OV (G47Δ) that is currently in clinical trial [A clinical study of a replication-competent, recombinant herpes simplex virus type 1 (G47Δ) in patients with progressive glioblastoma, http://apps.who.int./trailsearch/trail.aspx?trailid=JPRN-UMIN000002661] with angiostatin and characterized the efficacy of treating established intracranial gliomas with the combination of BEV and G47Δ-mAngio. We show that treatment of animals with BEV before injection of G47Δ-mAngio increases viral intratumoral distribution. This causes improved delivery of virus and angiostatin leading to a decrease in angiogenesis and tumor growth with increased survival. Moreover, G47Δ-mAngio decreases the invasive phenotypes induced by BEV.

RESULTS

Treatment of subcutaneous flank tumors with G47Δ-mAngio and G47Δ-empty

We first analyzed the efficiency of viral infection and angiostatin expression after G47Δ-mAngio injection in subcutaneous flank human U87 gliomas established in athymic mice. When the tumors reached a volume of 2 mm^3 they were treated with 5 × 10^6 plaque-forming unit (pfu) of G47Δ-mAngio or G47Δ-empty or an equal volume of phosphate-buffered saline (PBS). Tumors were collected 3 days after treatment for western blot analysis of virus-encoded angiostatin (hemagglutinin tag) and tumor VEGF expression (**Figure 1a**) and for histochemical analysis of viral distribution (LacZ) and tumor vascularity (CD31) (**Figure 1b**). G47Δ-empty slightly decreased tumor vascularity during the first 3 days of treatment, but expression of angiostatin by the virus had a very large antiangiogenic effect and decreased intratumoral VEGF levels, in agreement with previously published data[43] (**Figure 1**). At this time point ~10% of the tumor was infected with virus (**Figure 1b**).

Subcutaneous tumor models allow for sequential direct caliper measurements of tumor growth over time. Mice with established subcutaneous U87 tumors (2 mm^3) were treated twice (3 days apart) with 5 × 10^6 pfu of G47Δ-mAngio or G47Δ-empty or an equal volume of PBS (**Figure 2**). G47Δ-empty delayed the growth of subcutaneous tumors versus PBS but, importantly, angiostatin expression had significant therapeutic effect on tumor size by day 41 and it delayed tumor growth by 4 days compared with G47Δ-empty treated group (**Figure 2a**). The decrease in tumor vascularity mediated by angiostatin was still present weeks after the last viral treatment (**Figure 2b**).

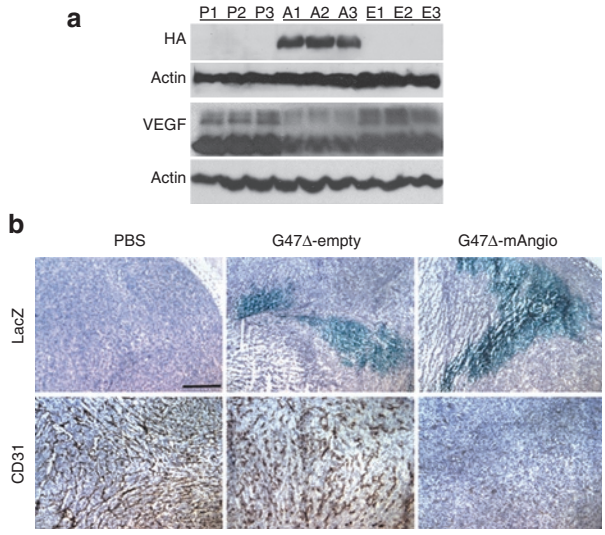

Figure 1 Virus-encoded angiostatin and tumor vascular endothelial growth factor (VEGF) expression and antiangiogenesis *in vivo*. (**a**) U87 flank tumors were harvested 3 days after treatment with phosphate-buffered saline (PBS) (P), G47Δ-mAngio (A), or G47Δ-empty (E) and analyzed by western blot for: angiostatin [hemagglutinin (HA) epitope], tumor VEGF, and β-actin (loading control). Each lane is a different mouse. (**b**) Histochemical staining for virus distribution (β-galactosidase activity, LacZ-blue) and tumor vascularity (CD31$^+$ brown) in tumors treated with PBS, G47Δ-empty, or G47Δ-mAngio (hematoxylin nuclear counterstaining). The bar indicates 2 mm. The analysis was done 3 days after treatment and 1 of 3 tumors/group is shown.

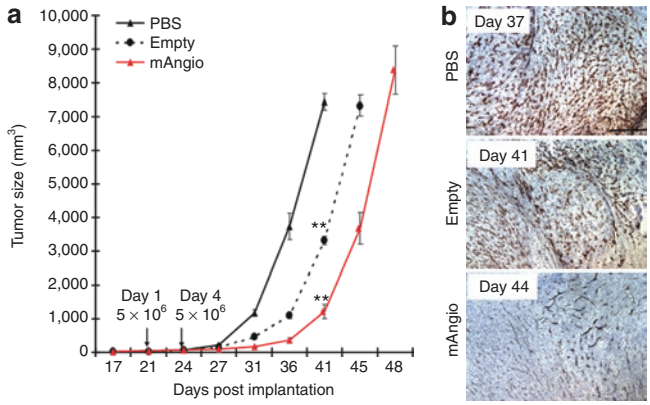

Figure 2 Treatment of subcutaneous flank tumors with G47Δ-mAngio and G47Δ-empty. (**a**) Growth (volume/days) of U87 tumors established subcutaneously in the flanks of athymic mice (N = 7/group). Virus (G47Δ-empty = empty or G47Δ-mAngio = mAngio) or phosphate-buffered saline (PBS) was injected on days 21 and 24 after tumor cell implantation. Significantly decreased growth was observed when the tumors were treated with G47Δ-empty compared to PBS (** referred to $P < 0.01$), and when treated with G47Δ-mAngio compared to G47Δ-empty ($P = 0.0002$) on day 41. (**b**) Staining for tumor vascularity (CD31$^+$ brown) at time of sacrifice: 17 days after treatment with PBS (37 days after tumor), 21 days after G47Δ-empty (41 days after tumor), or 24 days after G47Δ-mAngio (44 days after tumor). The bar indicates 2 mm.

© The American Society of Gene & Cell Therapy

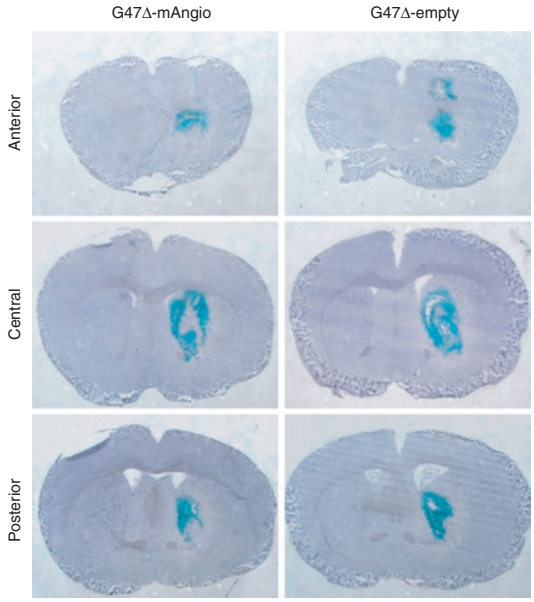

Figure 3 Virus infection of intracranial U87 tumors. Athymic mice with established intracranial U87 gliomas were treated with G47Δ-empty or G47Δ-mAngio (N = 3) injected directly into the tumor and sacrificed 6 hours later. Frozen brains were cut through the whole tumor area and analyzed for viral distribution. Lac Z staining (staining of viral β-galactosidase activity, blue) of two representative tumors treated with G47Δ-mAngio or G47Δ-empty at the anterior, central and posterior tumor area.

Pathologic analysis of intracranial tumors treated with BEV, G47Δ-mAngio, or G47Δ-empty

For a GBM therapy to be useful, it must ultimately be shown to work in an intracranial model. We have previously shown that athymic mice present an intact macrophage population that prevents intratumoral virus replication.[36,40,41] Thus, we decided to pursue our studies in athymic mice where human glioma tumors can be implanted. To analyze the effects of BEV, G47Δ-mAngio, and G47Δ-empty on intracranial U87 tumors, we performed histopathological analysis of the tumors extracted after treatment. We first compared the capacity of the two viruses to infect established intracranial U87 tumors. Six hours after virus injection, G47Δ-mAngio and G47Δ-empty infected intracranial U87 tumors with equal efficacy (~50–70% tumor infected, **Figure 3**).

We then performed more extensive immunohistochemical analysis of tumors treated with PBS, G47Δ-mAngio or G47Δ-empty alone, BEV alone, or the combination BEV + G47Δ-mAngio (**Figure 4a**). The brains were analyzed 3 days after intratumoral injection of 5×10^6 pfu virus or PBS, which corresponded to 5 days after intravenous injection of 5 mg BEV (5 mg/kg mouse) or PBS, for the presence of U87 cells (epidermal growth factor receptor), viral distribution (LacZ), vascularity (CD31), VEGF expression, and macrophage infiltration (F4/80) (**Figure 4a**). In parallel, RNA extracted from tumors treated with PBS, BEV, G47Δ-mAngio, and BEV + G47Δ-mAngio for 3 days was analyzed for expression of viral LacZ and tumor VEGF (**Figure 4b**). The dose of BEV was chosen from previously published data combining this drug with other OV strains.[42,44]

Comparison of intratumoral viral distribution at 6 hours (**Figure 3**) and 3 days (**Figure 4a**) after injection clearly shows that most of the injected virus has been cleared from the tumor, and the remaining virus is distributed exclusively around the borders between the tumor and the brain parenchyma (G47Δ-empty, **Figure 4a**). Angiostatin expression by the virus allowed persistence of a viral focus in the tumor center. This focus contained dead tissue without macrophages or vascularity, but was surrounded by an intense inflammatory area (**Figure 4a**).

G47Δ-empty decreased the vascularity of the tumor without affecting VEGF expression (**Figure 4a,b**). The tumor vascularity was further decreased by treatment with either BEV or G47Δ-mAngio alone, and the latter also decreased intratumoral VEGF expression (**Figure 4a,b**). G47Δ-empty infection was accompanied by the presence of dense active macrophages, whereas the areas of G47Δ-mAngio infection were characterized by necrosis (**Figure 4a**, black arrows) and decreased macrophage density (**Figure 4a**, F4/80 staining). BEV solo treatment also decreased the intratumoral macrophage density (**Figure 4a**) and combination of BEV with G47Δ-mAngio allowed increased distribution of virus during the first 3 days after injection, which was distributed almost through the entire tumor area, thus further decreasing the tumor vascularity and completely inhibiting macrophage intratumoral infiltration (**Figure 4a,b**). Increased viral activity induced by BEV was quantified through TaqMan reverse transcriptase-PCR performed on viral *LacZ* gene and on the tumor *VEGF* gene whose expression is suppressed by the angiostatin transgene (**Figure 4b**). Moreover, epidermal growth factor receptor staining of cancer cells clearly shows that almost all of the tumor has been killed by the virus when applied in combination with BEV (**Figure 4a**).

Altogether, BEV treatment decreased tumor vascularity and increased the oncolytic and antiangiogenic activity of G47Δ-mAngio, thus resulting in an improved antiangiogenic treatment effect further potentiated by the lysis of the tumor cells by the virus.

Survival of animals receiving BEV, G47Δ-mAngio, or G47Δ-empty as monotherapy

To determine whether the changes of the tumor and its microenvironment induced by G47Δ-mAngio, G47Δ-empty, or BEV treatment result in increased survival we performed Kaplan–Meier analysis of survival of mice with established U87 intracranial tumors.

We first compared the effects of G47Δ-mAngio versus G47Δ-empty, injecting 5×10^6 pfu of viruses per animal. Angiostatin expression by G47Δ significantly prolonged animal survival, with 40% of mice surviving over 150 days (**Figure 5a**). No distinct tumor mass and only very few tumor cells among an inflammatory region characterized by infiltrative neutrophils and macrophages were observed in the long-term survivors (**Figure 5b**).

We then tested the effects on animal survival of BEV at three different doses (**Figure 5c**): (i) the dose previously reported in combination with OV (5 mg/kg mouse injected twice a week for 4 weeks), (ii) the dose most frequently used when tested alone (10 mg/kg mouse injected twice a week for 4 weeks), and (iii) a higher dose (30 mg/kg mouse injected twice a week for 4

© The American Society of Gene & Cell Therapy

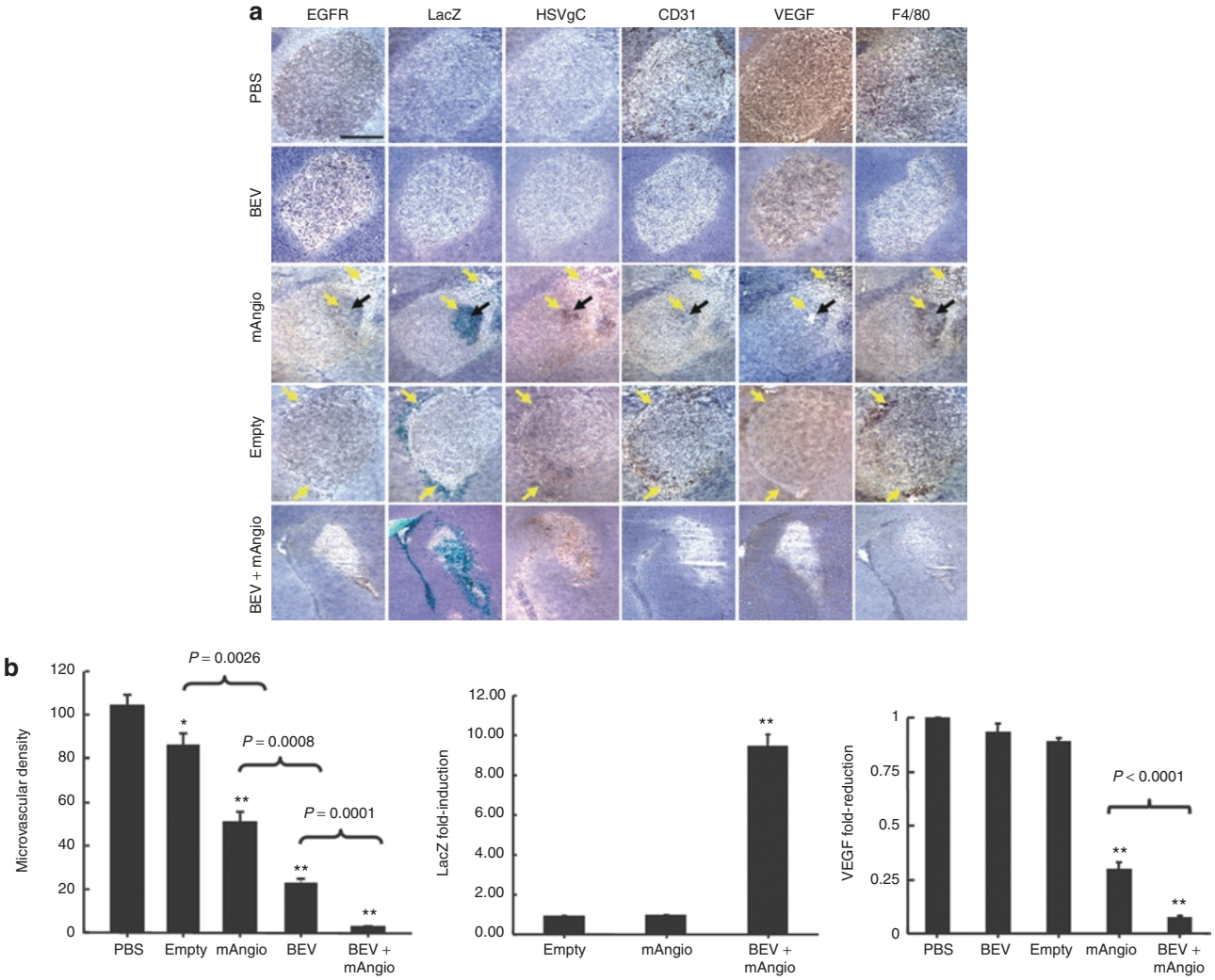

Figure 4 Tumor immunohistochemical analysis 3 days postvirus. (**a**) Sections of the central tumor area (hematoxylin nuclear counterstaining, purple) showing: tumor cells [epidermal growth factor receptor (EGFR), brown], viral distribution [HSVgC, brown and viral β-galactosidase activity (LacZ) blue], tumor vascularity (CD31, brown), vascular endothelial growth factor (VEGF) expression (VEGF, diffuse brown staining of the secreted molecule), and macrophage infiltration (F4/80, brown) in adjacent sections. The tumors were treated with: intratumoral (IT) phosphate-buffered saline (PBS) and intravenous (i.v.) PBS (PBS); IT PBS + i.v. BEV (BEV); IT G47Δ-mAngio + i.v. PBS (mAngio); IT G47Δ-empty + i.v. PBS (empty); IT G47Δ-mAngio + i.v. BEV (BEV + mAngio); $N = 3$. The yellow arrows indicate virus-infected areas. The black arrow indicates necrotic areas. (**b**) Left: intratumoral microvascular density in five treatment groups PBS, G47Δ-empty (empty), G47Δ-mAngio (mAngio), bevacizumab (BEV), BEV + G47Δ-mAngio (BEV + mAngio). On top of the bars, $^{*}P < 0.05$; $^{**}P < 0.01$, for each treatment compared to control (PBS), whereas P values on top of the connecting lines are for the indicated pair of treatments. Top right: Fold increase in viral LacZ mRNA in tumors treated with BEV + G47Δ-mAngio compared to those treated with G47Δ-mAngio alone (considered as baseline = 1). Bottom right: Tumor VEGF mRNA in animals treated BEV, G47Δ-mAngio and BEV + G47Δ-mAngio compared to control animals treated with PBS (considered as baseline = 1). $^{**}P < 0.01$ compared to control (PBS).

weeks). Monotherapy with BEV at 10 or 30 mg/kg increased animal survival when compared to treatment with 5 mg (which was already effective when compared to PBS-treated animals, Figure 5c). However, BEV treatment induced collagen deposits in the extracellular matrix[45] (an important extracellular factor to sustain adhesion of cancer cells during their invasion process) as well as expression of the invasion markers MMP2 and MMP9 (Figure 5d). Interestingly, tumors receiving the high doses of BEV (10 and 30 mg/kg mouse) also migrated to the extracranial region (data not shown). Conversely, tumors receiving only 5 mg/kg BEV had significantly less collagen deposits and decreased induction of MMP2 and MMP9 (Figure 5d); these tumors grew as circumscribed masses localized to the injection site, typical of the U87 model. No difference in survival was observed in mice receiving 10 versus 30 mg/kg of BEV (Figure 5c).

Combination of BEV with oHSV: survival and tumor response

To analyze the therapeutic benefits of the combination treatment BEV plus G47Δ-mAngio, we have compared this therapy to: (i) BEV plus G47Δ-empty, (ii) G47Δ-angio and G47Δ-empty alone, (iii) different doses of BEV alone. The combination treatment was done with the "noninvasive" BEV dose (5 mg/kg) and 10^6 pfu of oHSV. For this experiment, we have decreased the virus dose fivefold to avoid long-term survival induced by virus alone as was observed above. Animals treated with the combination

© The American Society of Gene & Cell Therapy

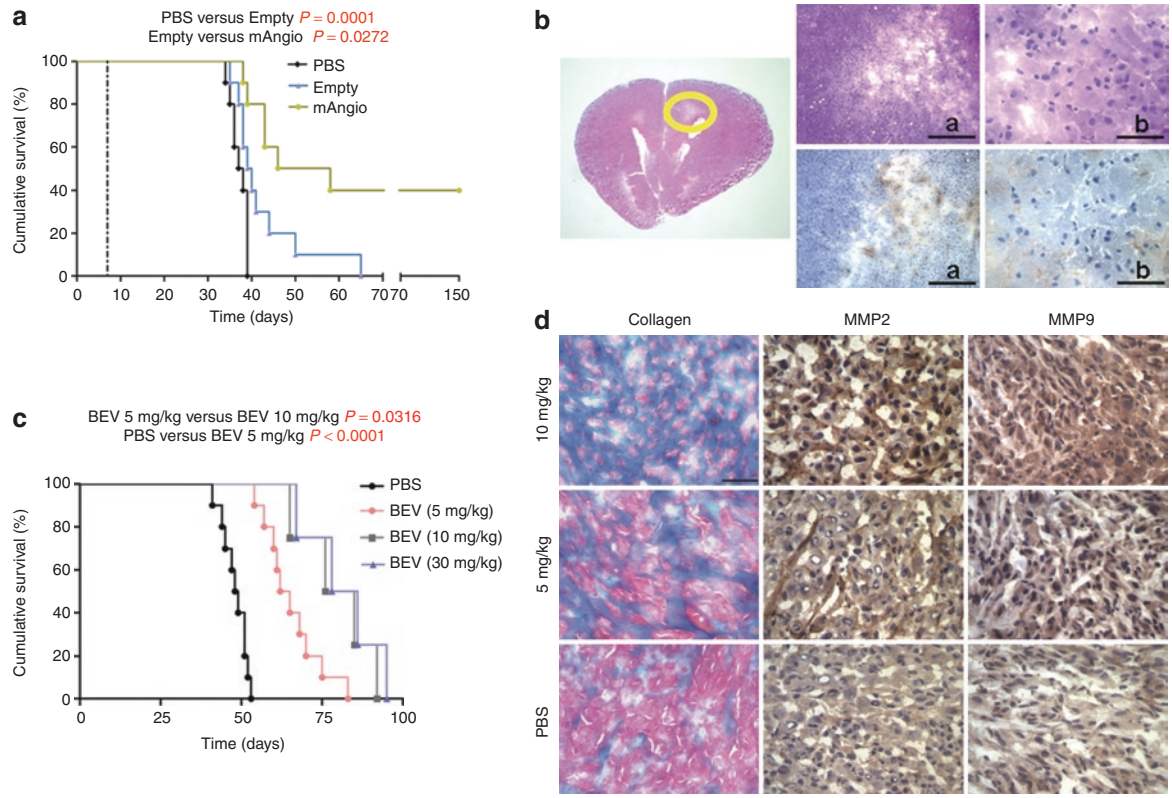

Figure 5 Kaplan–Meier analysis of survival with solo treatment. (**a**) Survival of mice with established U87 intracranial tumors treated intratumorally with phosphate-buffered saline (PBS), G47Δ-empty (empty), or G47Δ-mAngio (mAngio) ($N = 10$). The left dotted line indicates virus treatment on day 7. (**b**) Histopathologic analysis of a mouse brain carrying the U87 glioma and treated with G47Δ-mAngio (5×10^6 plaque-forming unit (pfu)/mice) that was still healthy after 150 days from tumor implantation. Same section at three different magnifications (The bar **a** indicates 2 mm, bar **b** indicates 0.5 mm), Left panel, the circle indicates the tumor area, right upper: hematoxylin and eosin (H&E); right lower: epidermal growth factor receptor (EGFR) (brown). (**c**) Survival of mice with established U87 intracranial tumors treated with different doses of intravenous (i.v.) bevacizumab (BEV) (5 mg, 10 mg, 30 mg BEV/kg). (**d**) Masson's trichrome staining for collagen deposits (blue) and immunohistochemistry staining for matrix metalloproteinase-2 (MMP2) and MMP9 expression (dark brown) in mice brain carrying the U87 glioma treated with PBS, 5 mg BEV/kg, 10 mg BEV/kg. The bar = 0.5 mm.

5 mg/kg BEV + G47Δ-mAngio survived longer than those receiving 5 mg BEV alone, G47Δ-angio alone, or 5 mg BEV + G47Δ-empty (**Figure 6a**). There was no statistically significant difference in survival between mice receiving BEV at 10 mg/kg versus BEV + G47Δ-empty or BEV + G47ΔmAngio. This may be due to the fact that animals with tumors growing partially in the extracranial region survive longer. Indeed, addition of G47Δ-mAngio to 5 mg/kg BEV completely inhibited the BEV-induced collagen deposits and decreased expression of MMP2 and MMP9 (**Figure 6b**), and tumors receiving this treatment did not migrate to the extracranial region.

To assess the orthotropic tumor response to the different treatments we performed serial magnetic resonance imaging (MRI), on two randomly selected mice for each treatment group from the survival experiment. T1-gadolinium MRI scans showed that whereas BEV has mainly a tumoristatic effect, the OV dramatically decreases the tumor size early in the course of treatment (**Figure 7a,b**). Of note, the MRI scans indicated the presence of small hemorrhagic foci (**Figure 7a**, arrow) in the tumors treated with G47Δ-mAngio. In addition, we did not observe any nonenhancing tumor formations by T2-weighted MRI when treating animals with only 5 mg/kg of BEV (data not shown).

DISCUSSION

We have tested the treatment efficacy of combining systemic BEV with local intratumoral injection of oHSV expressing angiostatin. The rationale for this combination is based on several foundations including: (i) Attacking angiogenesis via more than one mechanism; (ii) Previously published data showing that antiangiogenic treatments increase efficacy of OV by preventing intratumoral infiltration of macrophages that rapidly clear the virus from the tumor tissue;[39,41,42] and (iii) Previously published reports indicating that angiostatin inhibits migration not only of endothelial cells, but also of cancer cells, thus preventing tumor metastasis and invasion.[8,9] Indeed, one of the consequences of BEV therapy that prevents successful treatment of GBM is that it induces tumor invasion.

Specifically, our data show for the first time that: (i) in the noninvasive U87 intracranial glioma BEV induces proinvasive phenomena such as collagen deposits and expression of MMP2 and MMP9; (ii) BEV increases spread of oHSV and viral oncolytic activity by depleting intratumoral macrophages; (iii) arming oHSV with angiostatin provides increased antiangiogenic effects to the BEV treatment and decreases the proinvasive molecular changes induced by BEV; (iv) addition of oHSV armed with angiostatin

© The American Society of Gene & Cell Therapy

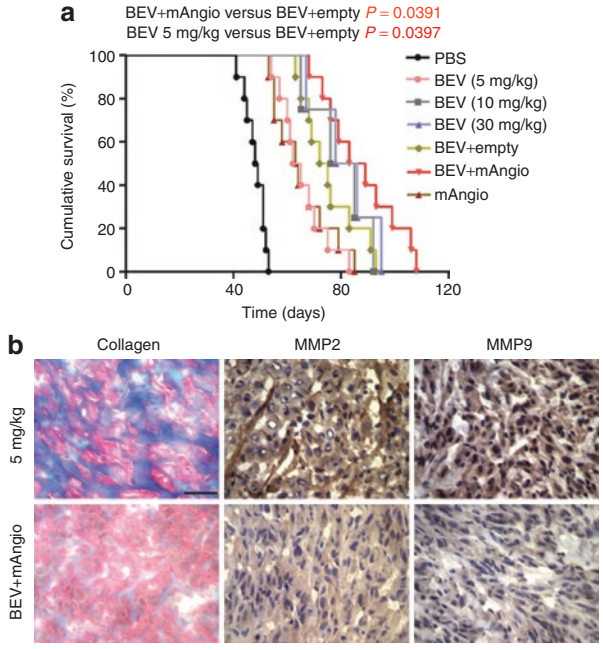

Figure 6 Kaplan–Meier analysis of survival with combination treatment. (**a**) Survival of mice treated with intratumoral (IT) phosphate-buffered saline (PBS) and i.v. PBS (PBS); IT PBS + i.v. BEV (bevacizumab (BEV), 5 mg/kg); IT PBS + i.v. BEV (BEV, 10 mg/kg); IT PBS + i.v. BEV (BEV, 30 mg/kg); IT G47Δ-empty + i.v. BEV (BEV+empty); IT G47Δ-mAngio + i.v. BEV (BEV+mAngio); and IT G47Δ-mAngio + i.v. PBS [mAngio, 1 × 10^6 plaque-forming unit (pfu)/mice]. The *P* values for each pair wise comparison are indicated. (**b**) Masson's trichrome staining for collagen deposits (blue) and immunohistochemistry staining for matrix metalloproteinase-2 (MMP2) and MMP9 expression (dark brown) in mice brain carrying the U87 glioma treated with 5 mg BEV/kg and IT G47Δ-mAngio + i.v. BEV (BEV+mAngio). The bar indicates 0.5 mm.

allows the use of decreased doses of BEV and reduces its unwanted invasive side effects. Previously published data indicate that BEV is most efficient in treating U87 intracranial tumors when used at 10 mg/kg mouse delivered twice a week for 4 weeks. However, at this or higher doses, BEV-induced invasion of U87 tumor, analogous to what observed in patients.[3,4] Accordingly, our data show that BEV alone does not cure U87 gliomas and no difference in survival was observed between 10 and 30 mg/kg. In addition, these high doses of BEV led to the development of tumors rich in invasion markers and migration of the cancer cells toward the extracranial regions. The lower dose of BEV (5 mg/kg) was less efficient in prolonging survival of animals with U87 tumors, but presented less collagen deposits and decreased induction of MMP2 and MMP9. These tumors also did not migrate to the extracranial region. Even though development of extracranial tumors is not by itself an indicator of tumor invasion, it is relevant that we have never observed this phenotype with the U87 cells, in the presence or absence of other treatments. Because BEV primarily inhibits activity of the human VEGF, which is synthesized by the tumor cells, the migration of U87 tumors to the extracranial region is most probably induced by BEV-mediated changes in the U87 glioma cells, rather than by modification of the mouse vascular and/or brain physiology. Moreover, this atypical behavior of U87 cells in mice corresponds to increased intratumoral markers of invasion. In this regard it is interesting to note that migration of cancer cells occurs by cellular attachment to the extracellular fibrin components, such as collagen, and concurrent directional collagen proteolysis mediated by a broad number of proteases including plasminogen activators.[46,47] Receptors for plasminogen activators are broadly expressed in GBM,[47] whereas contradictory data have been published about collagen deposits in these tumors.[48] However, a recent study indicates that *in vitro* treatment of U87 cells with BEV leads to increased expression of plasminogen, collagen as well as of MMP2 and MMP9 by these cells.[4] We thus believe that the migration of U87 tumors to the extracranial region is due to the invasive profile induced by BEV in these cancer cells and the atypical tumor environment provided by the mouse brain. Combination of 5 mg BEV/kg with an oHSV expressing angiostatin led to the same survival as BEV alone used at 10 or 30 mg/kg mouse, but collagen deposits were hardly observed in these tumors and there was no cancer migration to the extracranial region. For further improvement of this treatment it is important to define the mechanisms through which angiostatin inhibits BEV-induced collagen deposits, as well as MMP2 and MMP9 expression, and to test combination of G47Δ-mAngio with increased doses of BEV and with BEV delivered after OV injection, as previously described.[49]

In summary, these data present a therapeutic strategy with strong translational potential to the clinic, and suggest new avenues of exploration to improve intratumoral delivery of antiangiogenic proteins, to increase the oncolytic activity of cancer-selective viruses, and to decrease the toxicity of a promising drug recently approved for GBM treatment.

MATERIALS AND METHODS

Cell lines and cell culture. Monkey kidney cells (Vero) and U87 human glioma cells were purchased from American Type Culture Collection (Manassas, VA) and grown in complete Dulbecco's modified Eagle's medium supplemented with 10% fetal calf serum. Mouse endothelial cells MS1 were purchased from American Type Culture Collection and grown in RPMI medium supplemented with 10% fetal calf serum. Human umbilical vein endothelial cells were purchased from Lonza/Clonetics (Basel, Switzerland) and grown in endothelial growth medium-2 medium supplemented with the bullet kit provided by the company which includes 2% fetal bovine serum, heparin, hydrocortisone, ascorbic acid and the following human growth factors: fibroblast, vascular endothelial, R3-insulin, and endothelial. Human umbilical vein endothelial cells were maintained in culture for no >10 passages.

Viruses. The oHSV G47Δ, containing deletions of the γ34.5 and α47 genes and an inactivating insertion of *Escherichia coli* LacZ into ICP6, was armed with the mouse angiostatin complementary DNA tagged with the hemagglutinin epitope (G47Δ-mAngio) using the flip–flop HSV-BAC system (see **Supplementary Appendix**).

Animal studies. Female athymic nu/nu (NCI-Frederick nude) mice aged 6–8 weeks were obtained from NCI Frederick (Frederick, MD) and kept according to the guidelines of the Subcommittee on Research Animal Care of the Massachusetts General Hospital (Boston, MA). For brain tumor establishment, mice were injected stereotactically with 2 × 10^5 U87 cells (2 mm lateral to the bregma at a depth of 3 mm) in 2 µl PBS. Seven days after implantation tumors were injected with 5 × 10^6 pfu of virus resuspended in 2 µl of PBS or equivalent volume of PBS. Two hundred micro liter BEV (Avastin; Genentech, San Francisco, CA) was injected intravenously at 5, 10, or 30 mg/kg mouse twice a week for 4 weeks. Analysis of survival with the combination treatment (BEV+OV) was performed with 5 mg/kg mouse of BEV (starting 2 days before virus injection) and 10^6 pfu of virus or equivalent volume of PBS.

© The American Society of Gene & Cell Therapy

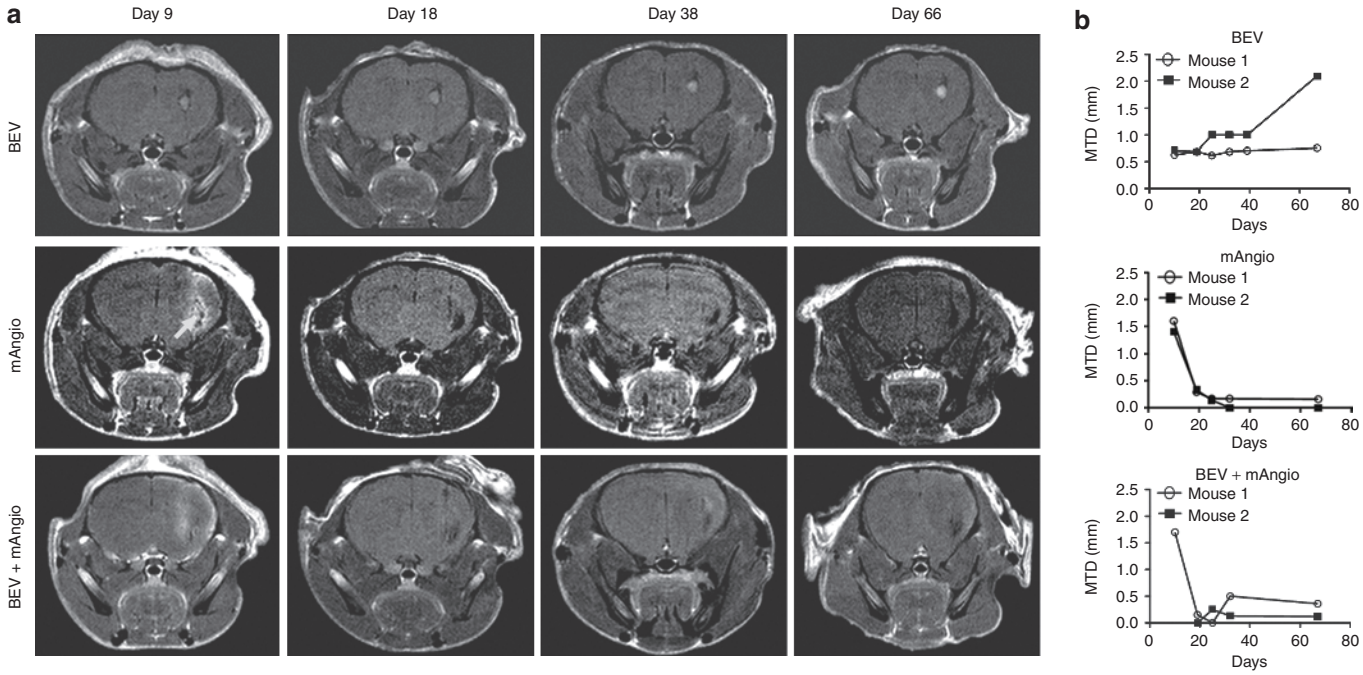

Figure 7 Magnetic resonance imaging (MRI) of treated tumors. (**a**) T1 scans of mice brains treated with bevacizumab (BEV) or G47Δ-mAngio (mAngio) alone or the combination BEV+G47Δ-mAngio (BEV + mAngio) at different time points after tumor implantation (the same mice as in **Figure 6**). The images show one mouse/treatment group of the two that were analyzed. Intravenous BEV treatment started on day 5 after tumor injection and was repeated twice a week for 4 weeks. G47Δ-mAngio was injected once into the tumor 7 days after implantation of U87 (*i.e.,* 2 days after BEV). The first image was taken 2 days after viral injection (9 days after tumor implantation). As shown in the survival analysis (**Figure 6**) the mice receiving treatments started dying shortly after day 54 from tumor implantation and imaging was thus discontinued. The arrow indicates hemorrhagic foci (it appeared also in the T2 scans before injection of Gd-DTPA, data not shown). (**b**) Quantitative representation of the images shown in **a**. Kinetics of tumor response (millimeters of maximum tumor diameter, MTD mm) is indicated in y-axis. The days from tumor implantation are indicated in x-axis (T1 scans of mouse 1 in each group is illustrated in **a**).

Flank tumors were obtained by injecting 2×10^5 U87 cells subcutaneously. When the tumors reached a volume of 2 mm^3 they received two injections 3 days apart of 5×10^6 pfu of virus or equivalent volume of PBS. Tumor volume was measured every 3–5 days and animals were sacrificed when the tumors reached a volume of 7–8 $\times 10^3$ mm^3.

Western blot. Tumors injected with the virus *in vivo* were homogenized into single-cell suspension in RIPA buffer (R0278; Sigma, St Louis, MO). Lysed with three freeze-thaw sonication cycles, and supernatants separated from insoluble pellets through centrifugation. Protein concentration of the supernatants was determined with the BCA kit (23227; Pierce, Rockford, IL) and analyzed by standard western blot after 12% SDS-polyacrylamide gel electrophoresis for the presence of chimeric mouse angiostatin-hemagglutinin protein (rat anti-hemagglutinin, 11867423001; Roche, Basel, Switzerland) and human VEGF (mouse antihuman VEGF, 555036, BD Biosciences, San Diego, CA).

Immunohistochemistry and Masson's trichrome staining. Rodent brains and flank tumors were removed and frozen in an isopentane dry-ice bath, then sectioned by cryostat to a thickness of 5 µm through the entire tumor volume. Every fifth section was collected for analysis. Tissue slides were dried overnight at room temperature, fixed in ice-cold acetone, and stored at –20 °C for hematoxylin and eosin (H&E) staining and immunohistochemistry analysis. The tissue slides were thawed and rehydrated in PBS before staining. The tumor was analyzed for cancer cells (human epidermal growth factor receptor), vascular density (CD31 antigen), macrophage infiltration (F4/80), and VEGF, MMP2, and MMP9 expression as follows: endogenous proteins and peroxidases were blocked with serum-free protein block (X0909) and peroxidase-blocking reagent (002428) (DAKO-Cytomation, Glostrup, Denmark). Mouse immunoglobulin G was blocked with mouse on mouse reagent (MKB2213; Vector Laboratories, Burlingame, CA). Sections were then incubated 1 hour at room temperature with each of the following primary antibodies: mouse antihuman epidermal growth factor receptor (M3563; Dako), rat anti-mouse CD31 (550274; BD Pharmingen, Franklin Lakes, NJ), rat anti-mouse F4/80 (MCA497RT; Serotec, Oxford, UK), mouse antihuman VEGF antibody (555036; BD Biosciences), rabbbit anti-matrix metalloproteinase-2 (MMP2) (ab37150; Abcam, Cambridge, MA), and rabbit anti-MMP9 (LS-B2486; LifeSpan Biosciences, Seattle, WA). This was followed by incubation with anti-rat or anti-mouse immunoglobulin G-HRP secondary antibody (ECL NA935V or NA931V; Amersham Pharmacia, Arlington Heights, IL). Liquid DAB Substrate Chromogen System (K3465; DAKO-Cytomation) was used for detection. Intratumoral G47Δ spread was analyzed through staining of viral β-galactosidase activity with X-gal reagent (5-bromo-4-chloro-3-inodolyl-β-D-galactopyranoside, B4252; Sigma) or immunohistochemistry staining for mouse anti HSV type 1 and 2 glycoprotein C (Serotec). β-Galactosidase staining was performed by adding an X-gal solution diluted to (0.4 mg/ml) of PBS to the acetone-fixed slides and incubated at 37 °C for 4 hours. Masson's trichrome staining (K037, Poly Scientific; R&D, Bayshore, NY) was conducted to localize collagen deposits. In all cases the sections were counterstained with hematoxylin, dehydrated with increasing concentrations of EtOH, and fixed in xylene. NIH ImageJ software was used to calculate the viral infected area in 10 different tumor slides cut across the whole tumor volume.

Quantitative reverse transcriptase-PCR. Total RNA from the tumor region of the cerebrum was extracted with the RNeasy Lipid Tissue kit (Qiagen, Valencia, CA) following manufacturer guidelines. complementary DNA was synthesized from 2 µg total RNA using the Omniscript Reverse

© The American Society of Gene & Cell Therapy

Transcriptase Kit (Qiagen, 205113) and random primers (Invitrogen, Carlsbad, CA). Quantitative, real-time, PCR was performed with the ABI Prism 7000 HT Sequence detection system and TaqMan (for lacZ) or SYBR-green (for VEGF and 18SrRNA) PCR Master Mixes (Applied Biosystems, Foster City, CA). The PCR reaction mix (25 µl) contained each primer at 0.9 µmol/l, the probe at 200 nmol/l, and 2 µl of diluted complementary DNA. The PCR program included 1 cycle of 2 minutes at 50 °C, 1 cycle of 10 minutes at 95 °C, and 40 cycles comprising 15 seconds at 95 °C followed by 1 minute at 60 °C. 18S rRNA was used as an internal control. Relative quantification of gene expression was calculated as $2\Delta^{Ct\ lacZ}/2\Delta^{Ct\ r18S}$, with Ct the number of cycles for saturation, and ΔCt the difference between the numbers of cycles needed to reach saturation for the same gene in two different treatment groups. The following primers were used: LacZ forward-TGTTGCCACTCGCTTTAATGAT, reverse-ACTCGCCGCA CATCTGAACT, probe-6FAM-CGCTGTACTGGAGGC-TAMRA; 18S rRNA forward-AACTTTCGATGGTAGTCGCCG, reverse-CCTTGGAT GTGGTAGCCGTTT; VEGF forward-CTACCTCCACCATGCCAAGT, reverse-TGGTGATGTTGGACTCCTCA.

MRI. MRI of mice brains was performed on a 4.7T MRI scanner (Bruker, Billerica, MA) with a dedicated mouse head coil under isofluorane anesthesia and respiratory monitoring. Sequential mouse axial T1-weighted images were acquired following intravenous administration of Gd-DTPA (Magnevist; Berlex, Montville, NJ), TR = 1100 ms, TE = 17 ms, FOV = 2.4 cm, matrix size = 256 × 192, slice thickness = 0.7 mm. Tumor sizes were obtained by measuring the maximum transverse dimension of the tumor. T2-weighted images were acquired before Gd-DTPA administration with similar parameters as above except TR = 3500 ms, TE = 86.8 ms, matrix size = 128 × 128.

Statistical analysis. Statistical analysis of animal survival was performed with log rank (Mantel–Cox) test, all other experiments were analyzed with two-sided ANOVA test followed by means comparisons with *post hoc* Tukey's test. $P < 0.05$ was considered to be statistically significant. All error bars indicate s.d.

SUPPLEMENTARY MATERIAL

Appendix.

ACKNOWLEDGMENTS

We thank Prof Xiang Zhang (Department of Neurosurgery, Xijing Hospital, P.R. China) and Prof Takashi Tamiya (Department of Neurological Surgery, Kagawa University Faculty of Medicine, Japan) for their great spiritual inspiration and editorial assistance. We thank Christopher J. Owen for his help in computer assistance. We thank the support from Postgraduate Scholarship Program of China Scholarship Council (CSC). This work was supported in part by grants from the National Institute for Neurological Disorders (R01-NS032677 to R.L.M., P30-NS045776 to S.D.R. for the real-time PCR core, U24CA092782 to R.W. for imaging core, R01-NS070835 and R01-NS072167 to J.W.C.) and the National Heart, Lung and Blood Institute (K08-HL081170 to J.W.C.) at the National Institutes of Health, USA. The authors declared no conflict of interest.

REFERENCES

1. Quesada, AR, Medina, MÁ, Muñoz-Chápuli, R and Ponce, ÁL (2010). Do not say ever never more: the ins and outs of antiangiogenic therapies. *Curr Pharm Des* **16**: 3932–3957.
2. Chamberlain, MC (2010). Emerging clinical principles on the use of bevacizumab for the treatment of malignant gliomas. *Cancer* **116**: 3988–3999.
3. de Groot, JF, Fuller, G, Kumar, AJ, Piao, Y, Eterovic, K, Ji, Y *et al.* (2010). Tumor invasion after treatment of glioblastoma with bevacizumab: radiographic and pathologic correlation in humans and mice. *Neuro-oncology* **12**: 233–242.
4. Lucio-Eterovic, AK, Piao, Y and de Groot, JF (2009). Mediators of glioblastoma resistance and invasion during antivascular endothelial growth factor therapy. *Clin Cancer Res* **15**: 4589–4599.
5. O'Reilly, MS, Holmgren, L, Shing, Y, Chen, C, Rosenthal, RA, Moses, M *et al.* (1994). Angiostatin: a novel angiogenesis inhibitor that mediates the suppression of metastases by a Lewis lung carcinoma. *Cell* **79**: 315–328.
6. Kirsch, M, Strasser, J, Allende, R, Bello, L, Zhang, J and Black, PM (1998). Angiostatin suppresses malignant glioma growth in vivo. *Cancer Res* **58**: 4654–4659.
7. Wahl, ML, Moser, TL and Pizzo, SV (2004). Angiostatin and anti-angiogenic therapy in human disease. *Recent Prog Horm Res* **59**: 73–104.
8. Perri, SR, Annabi, B and Galipeau, J (2007). Angiostatin inhibits monocyte/macrophage migration via disruption of actin cytoskeleton. *FASEB J* **21**: 3928–3936.
9. Stack, MS, Gately, S, Bafetti, LM, Enghild, JJ and Soff, GA (1999). Angiostatin inhibits endothelial and melanoma cellular invasion by blocking matrix-enhanced plasminogen activation. *Biochem J* **340**: 77–84.
10. Martuza, RL, Malick, A, Markert, JM, Ruffner, KL and Coen, DM (1991). Experimental therapy of human glioma by means of a genetically engineered virus mutant. *Science* **252**: 854–856.
11. Fulci, G and Chiocca, EA (2003). Oncolytic viruses for the therapy of brain tumors and other solid malignancies: a review. *Front Biosci* **8**: e346–e360.
12. Aghi, M, Rabkin, S and Martuza, RL (2006). Effect of chemotherapy-induced DNA repair on oncolytic herpes simplex viral replication. *J Natl Cancer Inst* **98**: 38–50.
13. Liu, TC, Castelo-Branco, P, Rabkin, SD and Martuza, RL (2008). Trichostatin A and oncolytic HSV combination therapy shows enhanced antitumoral and antiangiogenic effects. *Mol Ther* **16**: 1041–1047.
14. Post, DE, Fulci, G, Chiocca, EA and Van Meir, EG (2004). Replicative oncolytic herpes simplex viruses in combination cancer therapies. *Curr Gene Ther* **4**: 41–51.
15. Altomonte, J, Wu, L, Chen, L, Meseck, M, Ebert, O, García-Sastre, A *et al.* (2008). Exponential enhancement of oncolytic vesicular stomatitis virus potency by vector-mediated suppression of inflammatory responses in vivo. *Mol Ther* **16**: 146–153.
16. Altomonte, J, Wu, L, Meseck, M, Chen, L, Ebert, O, Garcia-Sastre, A *et al.* (2009). Enhanced oncolytic potency of vesicular stomatitis virus through vector-mediated inhibition of NK and NKT cells. *Cancer Gene Ther* **16**: 266–278.
17. Derubertis, BG, Stiles, BM, Bhargava, A, Gusani, NJ, Hezel, M, D'Angelica, M *et al.* (2007). Cytokine-secreting herpes viral mutants effectively treat tumor in a murine metastatic colorectal liver model by oncolytic and T-cell-dependent mechanisms. *Cancer Gene Ther* **14**: 590–597.
18. Fukuhara, H, Ino, Y, Kuroda, T, Martuza, RL and Todo, T (2005). Triple gene-deleted oncolytic herpes simplex virus vector double-armed with interleukin 18 and soluble B7-1 constructed by bacterial artificial chromosome-mediated system. *Cancer Res* **65**: 10663–10668.
19. Hardcastle, J, Kurozumi, K, Dmitrieva, N, Sayers, MP, Ahmad, S, Waterman, P *et al.* (2010). Enhanced antitumor efficacy of vasculostatin (Vstat120) expressing oncolytic HSV-1. *Mol Ther* **18**: 285–294.
20. Ino, Y, Saeki, Y, Fukuhara, H and Todo, T (2006). Triple combination of oncolytic herpes simplex virus-1 vectors armed with interleukin-12, interleukin-18, or soluble B7-1 results in enhanced antitumor efficacy. *Clin Cancer Res* **12**: 643–652.
21. Kaur, B, Cripe, TP and Chiocca, EA (2009). "Buy one get one free": armed viruses for the treatment of cancer cells and their microenvironment. *Curr Gene Ther* **9**: 341–355.
22. Li, X, Liu, YH, Lee, SJ, Gardner, TA, Jeng, MH and Kao, C (2008). Prostate-restricted replicative adenovirus expressing human endostatin-angiostatin fusion gene exhibiting dramatic antitumor efficacy. *Clin Cancer Res* **14**: 291–299.
23. Liu, G, Yuan, X, Zeng, Z, Tunici, P, Ng, H, Abdulkadir, IR *et al.* (2006). Analysis of gene expression and chemoresistance of CD133+ cancer stem cells in glioblastoma. *Mol Cancer* **5**: 67.
24. Malhotra, S, Kim, T, Zager, J, Bennett, J, Ebright, M, D'Angelica, M *et al.* (2007). Use of an oncolytic virus secreting GM-CSF as combined oncolytic and immunotherapy for treatment of colorectal and hepatic adenocarcinomas. *Surgery* **141**: 520–529.
25. Mullen, JT, Donahue, JM, Chandrasekhar, S, Yoon, SS, Liu, W, Ellis, LM *et al.* (2004). Oncolysis by viral replication and inhibition of angiogenesis by a replication-conditional herpes simplex virus that expresses mouse endostatin. *Cancer* **101**: 869–877.
26. Parker, JN, Meleth, S, Hughes, KB, Gillespie, GY, Whitley, RJ and Markert, JM (2005). Enhanced inhibition of syngeneic murine tumors by combinatorial therapy with genetically engineered HSV-1 expressing CCL2 and IL-12. *Cancer Gene Ther* **12**: 359–368.
27. Parker, JN, Pfister, LA, Quenelle, D, Gillespie, GY, Markert, JM, Kern, ER *et al.* (2006). Genetically engineered herpes simplex viruses that express IL-12 or GM-CSF as vaccine candidates. *Vaccine* **24**: 1644–1652.
28. Thorne, SH, Tam, BY, Kirn, DH, Contag, CH and Kuo, CJ (2006). Selective intratumoral amplification of an antiangiogenic vector by an oncolytic virus produces enhanced antivascular and anti-tumor efficacy. *Mol Ther* **13**: 938–946.
29. Tyminski, E, Leroy, S, Terada, K, Finkelstein, DM, Hyatt, JL, Danks, MK *et al.* (2005). Brain tumor oncolysis with replication-conditional herpes simplex virus type 1 expressing the prodrug-activating genes, CYP2B1 and secreted human intestinal carboxylesterase, in combination with cyclophosphamide and irinotecan. *Cancer Res* **65**: 6850–6857.
30. Tysome, JR, Briat, A, Alusi, G, Cao, F, Gao, D, Yu, J *et al.* (2009). Lister strain of vaccinia virus armed with endostatin-angiostatin fusion gene as a novel therapeutic agent for human pancreatic cancer. *Gene Ther* **16**: 1223–1233.
31. Yang, CT, Lin, YC, Lin, CL, Lu, J, Bu, X, Tsai, YH *et al.* (2005). Oncolytic herpesvirus with secretable angiostatic proteins in the treatment of human lung cancer cells. *Anticancer Res* **25**: 2049–2054.
32. Zamarin, D, Martínez-Sobrido, L, Kelly, K, Mansour, M, Sheng, G, Vigil, A *et al.* (2009). Enhancement of oncolytic properties of recombinant newcastle disease virus through antagonism of cellular innate immune responses. *Mol Ther* **17**: 697–706.
33. Friedman, A, Tian, JP, Fulci, G, Chiocca, EA and Wang, J (2006). Glioma virotherapy: effects of innate immune suppression and increased viral replication capacity. *Cancer Res* **66**: 2314–2319.
34. Fulci, G, Breymann, L, Gianni, D, Kurozomi, K, Rhee, SS, Yu, J *et al.* (2006). Cyclophosphamide enhances glioma virotherapy by inhibiting innate immune responses. *Proc Natl Acad Sci USA* **103**: 12873–12878.
35. Fulci, G, Dmitrieva, N, Gianni, D, Fontana, EJ, Pan, X, Lu, Y *et al.* (2007). Depletion of peripheral macrophages and brain microglia increases brain tumor titers of oncolytic viruses. *Cancer Res* **67**: 9398–9406.

© The American Society of Gene & Cell Therapy

36. Lamfers, ML, Fulci, G, Gianni, D, Tang, Y, Kurozumi, K, Kaur, B *et al.* (2006). Cyclophosphamide increases transgene expression mediated by an oncolytic adenovirus in glioma-bearing mice monitored by bioluminescence imaging. *Mol Ther* **14**: 779–788.
37. Lun, XQ, Jang, JH, Tang, N, Deng, H, Head, R, Bell, JC *et al.* (2009). Efficacy of systemically administered oncolytic vaccinia virotherapy for malignant gliomas is enhanced by combination therapy with rapamycin or cyclophosphamide. *Clin Cancer Res* **15**: 2777–2788.
38. Lun, XQ, Zhou, H, Alain, T, Sun, B, Wang, L, Barrett, JW *et al.* (2007). Targeting human medulloblastoma: oncolytic virotherapy with myxoma virus is enhanced by rapamycin. *Cancer Res* **67**: 8818–8827.
39. Otsuki, A, Patel, A, Kasai, K, Suzuki, M, Kurozumi, K, Chiocca, EA *et al.* (2008). Histone deacetylase inhibitors augment antitumor efficacy of herpes-based oncolytic viruses. *Mol Ther* **16**: 1546–1555.
40. Wakimoto, H, Fulci, G, Tyminski, E and Chiocca, EA (2004). Altered expression of antiviral cytokine mRNAs associated with cyclophosphamide's enhancement of viral oncolysis. *Gene Ther* **11**: 214–223.
41. Kurozumi, K, Hardcastle, J, Thakur, R, Yang, M, Christoforidis, G, Fulci, G *et al.* (2007). Effect of tumor microenvironment modulation on the efficacy of oncolytic virus therapy. *J Natl Cancer Inst* **99**: 1768–1781.
42. Libertini, S, Iacuzzo, I, Perruolo, G, Scala, S, Ieranò, C, Franco, R *et al.* (2008). Bevacizumab increases viral distribution in human anaplastic thyroid carcinoma xenografts and enhances the effects of E1A-defective adenovirus dl922-947. *Clin Cancer Res* **14**: 6505–6514.
43. Chung, AW, Hsiang, YN, Matzke, LA, McManus, BM, van Breemen, C and Okon, EB (2006). Reduced expression of vascular endothelial growth factor paralleled with the increased angiostatin expression resulting from the upregulated activities of matrix metalloproteinase-2 and -9 in human type 2 diabetic arterial vasculature. *Circ Res* **99**: 140–148.
44. Kottke, T, Hall, G, Pulido, J, Diaz, RM, Thompson, J, Chong, H *et al.* (2010). Antiangiogenic cancer therapy combined with oncolytic virotherapy leads to regression of established tumors in mice. *J Clin Invest* **120**: 1551–1560.
45. Provenzano, PP, Eliceiri, KW, Campbell, JM, Inman, DR, White, JG and Keely, PJ (2006). Collagen reorganization at the tumor-stromal interface facilitates local invasion. *BMC Med* **4**: 38.
46. Friedl, P and Wolf, K (2008). Tube travel: the role of proteases in individual and collective cancer cell invasion. *Cancer Res* **68**: 7247–7249.
47. Gondi, CS, Lakka, SS, Yanamandra, N, Olivero, WC, Dinh, DH, Gujrati, M *et al.* (2004). Adenovirus-mediated expression of antisense urokinase plasminogen activator receptor and antisense cathepsin B inhibits tumor growth, invasion, and angiogenesis in gliomas. *Cancer Res* **64**: 4069–4077.
48. Huijbers, IJ, Iravani, M, Popov, S, Robertson, D, Al-Sarraj, S, Jones, C *et al.* (2010). A role for fibrillar collagen deposition and the collagen internalization receptor endo180 in glioma invasion. *PLoS ONE* **5**: e9808.
49. Eshun, FK, Currier, MA, Gillespie, RA, Fitzpatrick, JL, Baird, WH and Cripe, TP (2010). VEGF blockade decreases the tumor uptake of systemic oncolytic herpes virus but enhances therapeutic efficacy when given after virotherapy. *Gene Ther* **17**: 922–929.